Computer Methods and Programs in Biomedicine 158 (2018) 41–52

Contents lists available at ScienceDirect

Computer Methods and Programs in Biomedicine

journal homepage: www.elsevier.com/locate/cmpb

Segmentation of liver and vessels from CT images and classification of liver segments for preoperative liver surgical planning in living donor liver transplantation

Xiaopeng Yang[a], Jae Do Yang[b,c,d], Hong Pil Hwang[b,c,d], Hee Chul Yu[b,c,d,*], Sungwoo Ahn[b,c,d], Bong-Wan Kim[e], Heecheon You[a]

[a] Department of Industrial Management and Engineering, Pohang University of Science and Technology, Pohang, 37673, South Korea
[b] Department of Surgery, Chonbuk National University Medical School, Jeonju, 54907, South Korea
[c] Research Institute of Clinical Medicine of Chonbuk National University-Biomedical Research Institute of Chonbuk University Hospital, Jeonju, 54907, South Korea
[d] Research Institute for Endocrine Sciences, Chonbuk National University, Jeonju, 54907, South Korea
[e] Department of Liver Transplantation and Hepatobiliary Surgery, Ajou University School of Medicine, Suwon, 16499, South Korea

ARTICLE INFO

Article history:
Received 16 March 2017
Revised 13 November 2017
Accepted 11 December 2017

Keywords:
Liver segmentation
Vessel segmentation
Automatic segmentation
Liver segment classification
Living donor liver transplantation

ABSTRACT

Background and objective: The present study developed an effective surgical planning method consisting of a liver extraction stage, a vessel extraction stage, and a liver segment classification stage based on abdominal computerized tomography (CT) images.
Methods: An automatic seed point identification method, customized level set methods, and an automated thresholding method were applied in this study to extraction of the liver, portal vein (PV), and hepatic vein (HV) from CT images. Then, a semi-automatic method was developed to separate PV and HV. Lastly, a local searching method was proposed for identification of PV branches and the nearest neighbor approximation method was applied to classifying liver segments.
Results: Onsite evaluation of liver segmentation provided by the SLIVER07 website showed that the liver segmentation method achieved an average volumetric overlap accuracy of 95.2%. An expert radiologist evaluation of vessel segmentation showed no false positive errors or misconnections between PV and HV in the extracted vessel trees. Clinical evaluation of liver segment classification using 43 CT datasets from two medical centers showed that the proposed method achieved high accuracy in liver graft volumetry (absolute error, AE = 45.2 ± 20.9 ml; percentage of AE, %AE = 6.8% ± 3.2%; percentage of %AE > 10% = 16.3%; percentage of %AE > 20% = none) and the classified segment boundaries agreed with the intraoperative surgical cutting boundaries by visual inspection.
Conclusions: The method in this study is effective in segmentation of liver and vessels and classification of liver segments and can be applied to preoperative liver surgical planning in living donor liver transplantation.

1. Introduction

Extraction of the liver and vessels from computerized tomography (CT) images and division of the liver into segments are essential for planning a safe living donor liver transplantation (LDLT) surgery. The complex liver anatomy structures consisting of the pipeline systems of hepatic artery, portal vein (PV), hepatic vein (HV), and bile duct and their variations result in the complexity, difficulty, and risk of liver surgery [1]. A comprehensive surgery plan in consideration of vascular structures and their anatomical relationships with the liver segments is of help to ensure a safe liver resection [1–6].

Various liver segmentation algorithms can be classified into manual, semi-automatic, and automatic methods. Tracing a liver contour on each CT slice by mouse clicking, a manual method provides most accurate segmentation but is cumbersome and time demanding(>30 min) to users [7]. In contrast, an automatic method segments the liver without user interaction [8–11], but sacrifices accuracy [12]. For example, Wu et al. [9] proposed an automatic segmentation method using supervoxel-based graph cuts, resulting in an average overlap accuracy of 92.1% and an average

* Corresponding author at: Department of Surgery, Chonbuk National University Medical School, Jeonju, 54907, South Korea
E-mail address: hcyu@jbnu.ac.kr (H.C. Yu).

https://doi.org/10.1016/j.cmpb.2017.12.008
0169-2607/

processing time of 27 s per CT dataset (CT slice thickness: 1 to 3 mm) on a computer with an Intel Core CPU 2.40 GHz processor. Lastly, a semi-automatic method extracts the liver starting from predefined seed points or regions, resulting in a higher accuracy but a longer processing time than an automatic method. For example, Peng et al. [13] proposed a multiregion-appearance based approach with graph cuts to segment the liver from a manual initialization of cylinders at different CT slices, resulting in an average overlap accuracy of 95.4% and an average computation time of 3 min for a CT dataset of 180 slices without including times of preprocessing, initialization, and postprocessing on a computer with an Intel Core i5-4200 U CPU 1.60 GHz processor.

Next, vessel segmentation algorithms can be grouped into semi-automatic and fully automatic methods. A semi-automatic extraction method segments vessel structures starting from selected seed points or regions by iteratively adding adjacent structures that satisfy certain segmentation criteria. For example, Selle et al. [14] applied a region growing method to segment liver vessels with automatically adjusted thresholds, but their method has a limitation in segmenting small vessels [15]. Yi and Ra [16] proposed a locally adaptive region growing method to segment vessel trees, in which locally adaptive analysis was repeatedly performed throughout the whole image to identify small vessels and therefore not efficient. Lorigo et al. [17] applied a level-set method to vessel segmentation with an initialization and a speed function. In contrast to a semi-automatic method, a fully automatic method extracts vessel structures based on statistical histogram analysis or a local shape descriptor such as a tube detection filter. For example, Soler et al. [18] estimated thresholds based on an intensity histogram to extract vessels with a morphological closing step and then removed false branches by analyzing the skeletonized vessel structures. Eidheim et al. [19] used a matched filter to enhance vessel structures and then a generic algorithm for globally searching target vasculatures.

The conventional semi-automatic and fully automatic methods have difficulties in dealing with local disturbances such as low contrast or connected structures with similar intensity values. To overcome the limitations of the conventional methods, Esneault et al. [15] applied Boykov's graph cuts algorithm to segment liver vessels, claiming that the PV and HV were naturally separated in their experiments. Bauer et al. [20] proposed a two-step method to separate and segment interwoven tubular tree structures: (1) identification of tubular objects and (2) grouping different tree structures followed by graph cuts for segmentation.

Abdominal images scanned using magnetic resonance imaging (MRI) technique have been increasingly used in clinic because no radiation is involved in obtaining MRI images and bile duct is clearly visible in MRI images. Segmentation of the liver and vessels from MRI images has been studied recently [21–26] though it is still challenging to extract vessels from MRI images due to lower image quality than CT images. For example, Goceri et al. [25] proposed a fully automatic level set based method for liver segmentation from MRI images and Goceri [21] developed an automated labeling method for extraction of PV and HV based on the gray-level values and anatomical structures of the vessels. However, CT images are still mainly used as a routine clinical examination due to the lower cost, shorter scanning time, and higher image quality of CT images than MRI images. The present study aimed at improving our previous hybrid semi-automatic method [12] on CT images in terms of accuracy and time efficiency.

Lastly, methods for classification of liver segments can be categorized into plane-based and model-based methods. A plane-based method divides the liver into different segments by several planes that pass through PV and HV [27–29]. For example, Oliveira et al. [29] used three vertical planes generated by selected voxels from the left, meddle, and right HV branches and one horizontal plane generated by the selected voxels from PV to divide the liver into eight Couinaud segments [30]. However, a plane-based method is not appropriate for practical application in a clinical environment due to a significant difference of their flat plane segment boundaries from corresponding true curved segment boundaries. Next, a model-based method identifies PV branches for each of eight liver segments and then assign each voxel to one of the liver segments if the blood supply of the voxel is provided by the PV branches of that segment [14,31]. To determine the blood supply of a voxel in a model-based method, Laplacian approximation (LA) and nearest neighbor approximation (NNA) approaches were proposed and evaluated by Selle et al. [14]. The LA method calculates potential values of a voxel to PV branches by solving Laplacian equations for the eight liver segments and classifies the voxel to a liver segment of which corresponding potential value is largest. The NNA method calculates the Euclidean distances of a voxel to PV branches for the eight liver segments and classifies the voxel to a liver segment of which corresponding distance is shortest. Selle et al. [14] compared the performance of the LA and NNA methods and found that the NNA method (accuracy = 89.9%) slightly outperformed the LA method (accuracy = 88.6%) in liver segment classification. However, in both the LA and NNA methods, interactive identification of PV branches for the eight liver segments is a challenging task due to difficulty in selecting a root point for identification of PV branches in 3D.

Commercial software solutions of companies including Philips, Siemens, and Fujifilm which provide automatic segmentation of the liver and vessels and semi-automatic resection planning of liver surgery have become available. However, the technical details of their automatic segmentation algorithms are not publically available, which makes it hard to recognize their features, advances, and limitations from theoretical and/or methodological aspects.

The present study was intended to develop an effective surgical planning method, which consists of a liver extraction stage, a vessel extraction stage, and a liver segment classification stage using abdominal CT images. An automatic seed point identification method, customized level set methods, and an automated thresholding method were applied in this study to extraction of the liver and vessels from CT images. Then, a semi-automatic method was developed to separate PV and HV. Lastly, a local searching method was proposed for identification of PV branches and the NNA method was applied to classification of liver segments. The effectiveness of the proposed surgical planning method was evaluated in three steps: (1) onsite evaluation of liver segmentation provided by the SLIVER07 website, (2) expert evaluation of vessel segmentation in terms of false positive error, false negative error, and connection between PV and HV, and (3) clinical evaluation of liver segment classification in terms of liver graft volumetry accuracy and visual comparison of the classified liver segment boundaries to the corresponding intraoperative surgical cutting boundaries.

2. Surgical planning method development

The surgical planning method for LDLT consists of three steps: (1) segmentation of the liver using an automatic seed point identification method and customized level set methods (2) segmentation of PV and HV using a region growing method from automatically identified seed points and threshold intervals, and (3) identification of PV branches and classification of liver segments from the identified PV branches using the NNA method.

2.1. Liver extraction

An automatic liver segmentation method was developed based on Yang et al. [12]'s hybrid semi-automatic liver segmentation

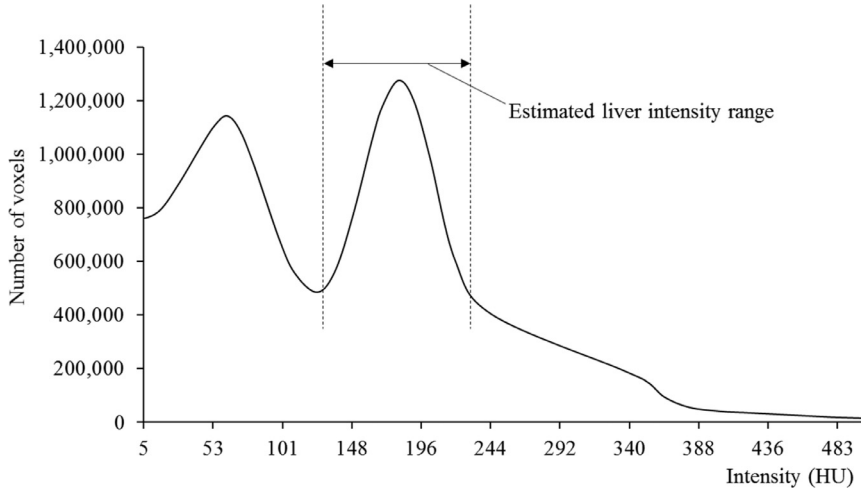

Fig. 1. Estimation of the intensity range of liver in a histogram.

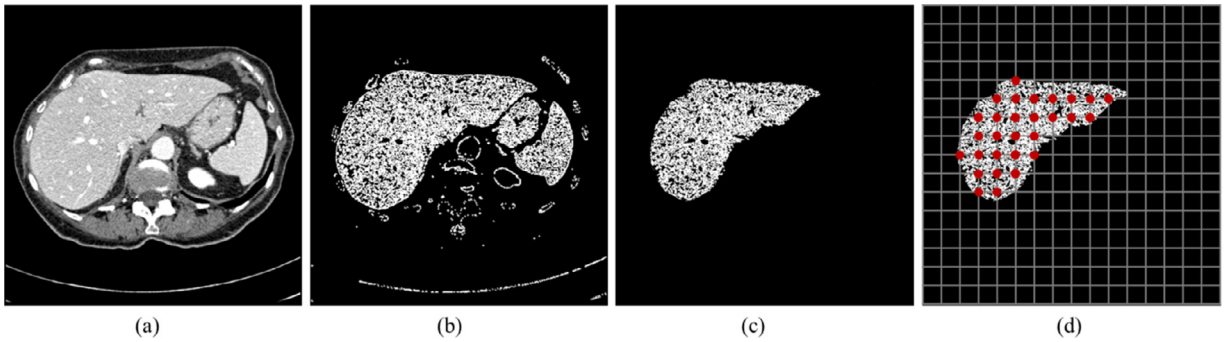

Fig. 2. Automatic identification of seed points for liver segmentation: (a) original image, (b) binary image created based on an intensity range of the liver estimated by histogram analysis, (c) liver region after removing small objects and erosion of the binary volume by five pixels, (d) seed points identified from the nodes inside the liver region in a 16×16 grid.

method by adding a histogram analysis of intensity values and a geometric analysis of the liver for automatic identification of seed points from CT images. Automatic identification of seed points is added as a new feature to avoid an interactive selection of seed points over CT images which takes about 30 s in the hybrid method. Ruskó et al. [7] reported that the liver is the largest organ and mostly located on the right side of human body. A histogram of voxels located on the right side of the body is constructed and smoothed using the *sgolayfilt* function (polynomial order = 3; frame length = 27) in Matlab R2011a (MathWorks Inc., Natick: MA, USA) to find the average intensity of liver voxels. Two significant maxima appear in the smoothed histogram (Fig. 1) in which the larger maxima belongs to the liver and the other to muscles [7]. Lastly, the minimal and maximal intensity values of liver voxels are estimated by finding large changes in the derivatives of the histogram (Fig. 1).

A binary volume is created by assigning the intensity values of voxels inside the minimal and maximal liver intensity range as one and the rest outside the range as zero (Fig. 2.b). Objects in the binary volume are then identified by the connected component analysis method in ITK [32]. Among the identified objects, the liver belongs to the largest object because the liver is the largest organ [7]. The largest object is retained for further processing and other objects are removed. The largest object is then eroded using the binary erode image filter [36,37] in ITK [32] by five pixels determined by an exhaustive experiment to further remove any falsely identified objects that do not belong to the liver (Fig. 2.c). Five to six slices are selected every 40 slices in the binary volume as candidates for seed point identification. Lastly, a 16×16 grid is generated over the selected slices on which the nodes having an intensity of one are considered as seed points for liver segmentation (Fig. 2.d).

After automatic identification of multiple seed points, the automatic liver segmentation method incorporates a customized fast-marching level set method [33] for formation of an initial liver region and a threshold-based level set method [34,35] for detection of the actual liver region from the initial liver region. The customized fast-marching level set method consists of four steps: (1) calculation of gradient magnitude at each voxel, (2) calculation of a contour propagation speed based on the gradient magnitude at each voxel, (3) calculation of an arrival time of the propagation contour at each voxel, and (4) generation of an initial liver region based on the calculated arrival times. The initial liver region is then propagated to reach the actual liver boundary by the threshold-based level-set method. Holes in the extracted liver are filled using the binary morphological closing image filter in ITK [32,38]. Then the extracted liver is smoothed by a binary median smoothing filter. More detailed information of the customized fast-marching level set method, the threshold-based level set method, and the smoothing method can be found in our previous paper [12].

The liver with tumors was segmented by including the tumors to the extracted liver using a hole filling method to fill the holes of the tumors caused by the intensity differences between the tumors and the liver tissues in the extracted liver. As illustrated in Fig. 3, different methods were applied for inclusion of tumor regions into the extracted liver depending on whether a tumor region is open or closed. In case of a closed tumor region (Fig. 3a), the tumor is

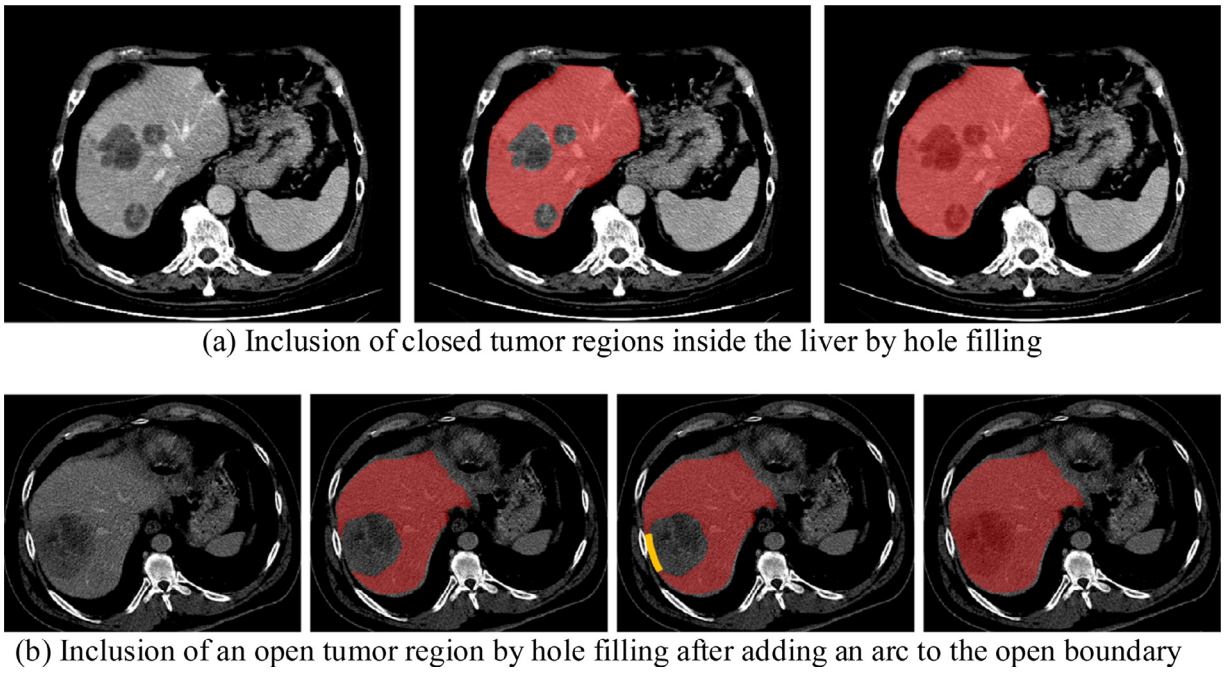

Fig. 3. Inclusion of tumor regions to the extracted liver region.

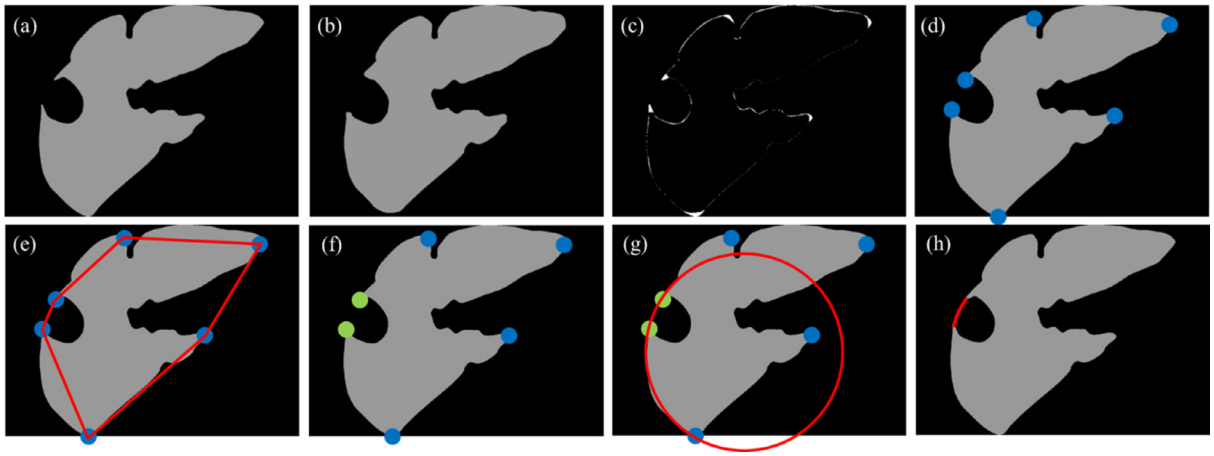

Fig. 4. Formation of an arc in liver segmentation (illustrated): (a) original liver region with an open tumor region at the right liver lobe, (b) smoothed liver region, (c) subtraction of the smoothed liver region from the original liver region, (d) corners found in the liver boundary, (e) boundary lines connecting the identified corners, (f) two corners identified on the open tumor region, (g) a circle passing through the identified corners and fit to the liver boundary near the open tumor region, (h) an arc formed from the circle.

added to the extracted liver by hole filling. In contrast, in case of an open tumor region (Fig. 3b; a tumor is located at the boundary of the liver), an arc is automatically drawn slice by slice using the arc generation method proposed by Abdel-massieh [11] to form a closed tumor region and then the tumor region is added to the extracted liver by hole filling. The arc generation method consists of (1) finding corners located on the liver boundary by subtracting the smoothed liver region from the original liver region (Fig. 4.a–d), (2) identifying two corners on the open tumor region at which a line connecting the two corners completely lies outside the liver region and a vacant region exists inside the line (Fig. 4.e,f), and (3) forming an arc connecting the identified corners from a circle passing through the two corners and fit to the liver boundary near the open tumor region (Fig. 4.g,h).

2.2. Vessel extraction

PV and HV were extracted from CT images in five steps: (1) masking CT images with the extracted liver region, (2) identification of seed points, (3) identification of multiple threshold intervals, (4) vessel extraction by a customized region growing method and selection of the most appropriate candidate among the extractions from different threshold intervals, and (5) separation of PV and HV. In the CT masking stage, CT images were masked using the extracted liver region to remove surroundings of the liver to avoid false extraction of vessels outside the liver and reduce vessel extraction time (Fig. 5). In the seed point identification stage, a similar method employed to liver extraction was used for automatic identification of seed points for vessel extraction. A histogram of the masked CT images was calculated to find the average intensity of vessel voxels. Two significant maxima appear in the histogram in which the larger maxima belongs to the vessels and the other to

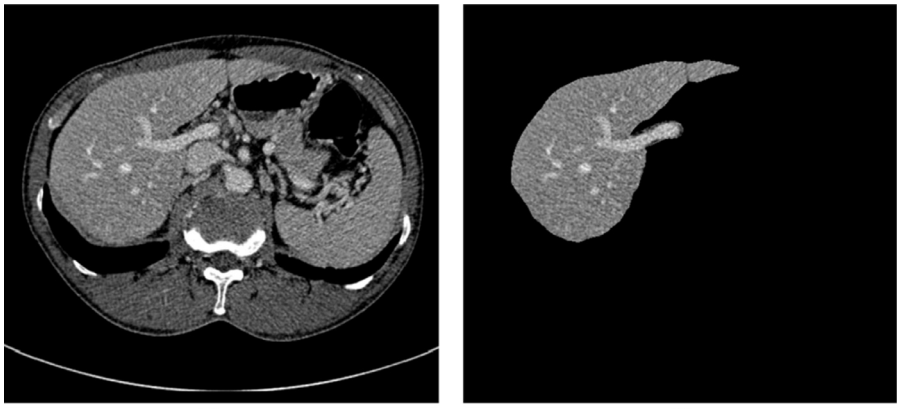

Fig. 5. Masking a CT image with an extracted liver region to remove surroundings of the liver for vessel extraction: (a) original image and (b) masked image.

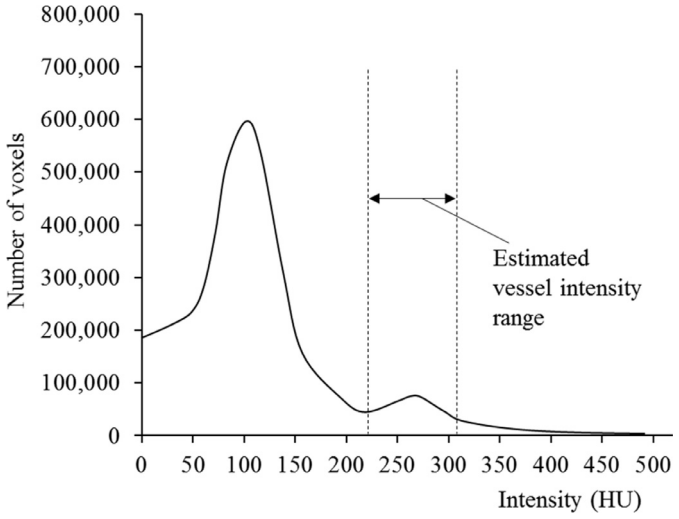

Fig. 6. Estimation of the intensity range of liver vessels in a histogram.

the liver (Fig. 6). The minimal and maximal intensity values of vessel voxels are estimated by finding large changes in the derivatives of the histogram (Fig. 6). Then a similar seed point identification procedure to liver extraction is applied to identify seed points for vessel extraction.

In the threshold interval identification stage, threshold intervals are calculated based on the average value (μ) and standard deviation (σ) of vessel intensity values (calculated from the identified seed points) by $[\mu - a\sigma,\ \mu + b\sigma]$, where a and b are parameters to be determined empirically. An exhaustive experiment was conducted to find appropriate values for a and b which maximize the accuracy of vessel extraction using 30 training CT datasets (10 having no tumors from a medical center with a slice thickness of 1 mm; 20 having tumors, lesions, and cysts with different sizes, shapes, and locations in most cases from the SLIVER07 website with a slice thickness from 0.7 to 5.0 mm). The accuracy of vessel extraction was assessed by an expert radiologist. The space for finding appropriate parameter values was narrowed down consisting of $5 \times 5 \times 30$ trials of vessel extraction (a and b: $1.0 \sim 3.0$ with an interval of 0.5) after exhaustive experiments. Appropriate values of average $\pm$ S.D. found for a and b were 1.4 ± 0.4 (range = 1.0 to 2.0) and 3.0 ± 0.0, respectively. Six threshold intervals, $[\mu - 1.0\sigma,\ \mu + 3.0\sigma]$, $[\mu - 1.2\sigma,\ \mu + 3.0\sigma]$, $[\mu - 1.4\sigma,\ \mu + 3.0\sigma]$, $[\mu - 1.6\sigma,\ \mu + 3.0\sigma]$, $[\mu - 1.8\sigma,\ \mu + 3.0\sigma]$, and $[\mu - 2.0\sigma,\ \mu + 3.0\sigma]$ were then identified as candidates for vessel extraction.

In the vessel extraction stage, PV and HV are extracted using a connected threshold region growing method in ITK [32] from the identified seed points and six threshold intervals. Starting from the identified seed points, the region growing method searches neighboring voxels and adds voxels to the extracted vessels if the voxels are in the given threshold intervals. An interface (Fig. 7) was provided for the user to verify and select the most appropriate vessel extraction result. Six candidates extracted from the smallest to the largest threshold intervals were sequentially shown to the user with volume information. Checkboxes were provided for the user to select the most appropriate extraction result.

Lastly, in the PV and HV separation stage, PV and HV are separated by a connected component analysis method. After extraction of the vessels, connected branches were identified by the connected component analysis method in ITK [32]. In the case that PV and HV are connected with each other, a scalable 3D sphere is provided for the users to separate PV and HV by removing the voxels connecting PV and HV with the sphere. Branches belonging to PV are then interactively selected with an interface (Fig. 8) to separate PV and HV.

2.3. Classification of liver segments

Liver segments are classified in three steps: (1) skeletonization of PV, (2) identification of PV branches for each liver segment, and (3) division of the liver into eight segments based on the identified PV branches. In the PV skeletonization stage, PV is skeletonized by a 3D binary thinning method [39]. The binary thinning method symmetrically erodes the PV surface iteratively until only the skeleton remains while preserving the medial position of the skeleton lines and connectedness of PV branches. For example, Fig. 9a illustrates a skeletonized PV tree generated using the 3D binary thinning method.

In the PV branch identification stage, a local searching method was developed to select a root point on a target PV branch in 3D to assign the PV branch to its corresponding liver segment. The local searching method consists of three steps: (1) clicking the root point on the target PV branch, where the picked point might be different from the root point due to a lack of depth perception. (2) searching neighboring points around the picked point with a radius of 5 pixels determined by an exhaustive experiment and identifying those points located on the PV branch, and (3) among the identified points, finding the root point which is the closest point to the picked point (Fig. 10):

$$P_j = \text{root point if } D(P_j) = \min_{i=1,\ldots,N} \{D(P_i)\} \quad (1)$$

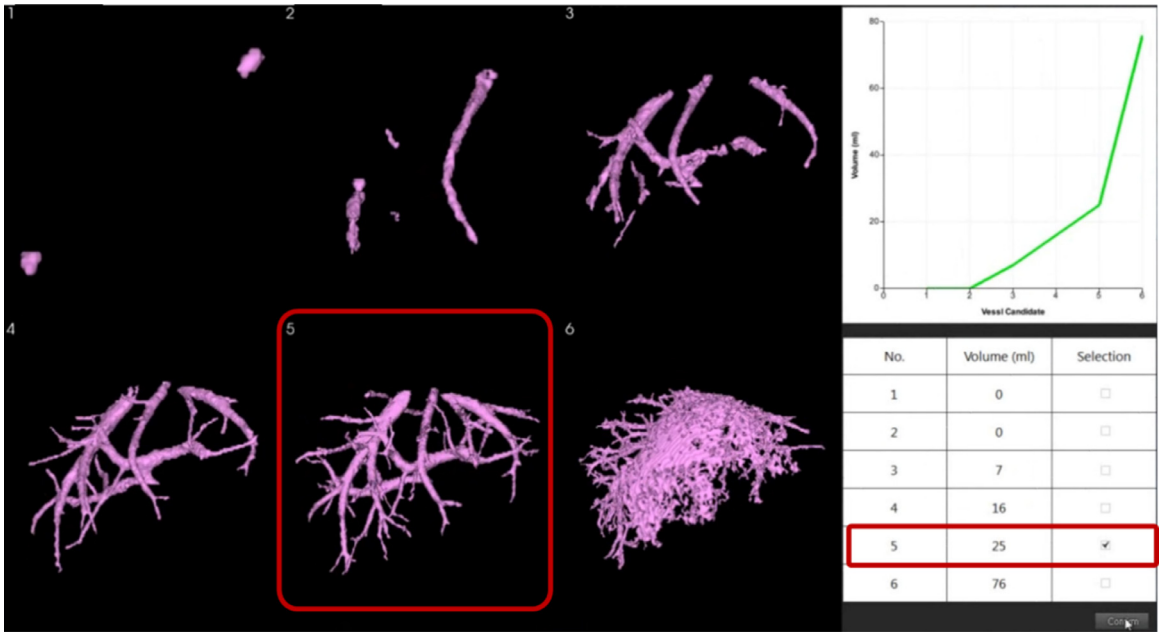

Fig. 7. An interface for the user to verify and select an appropriate vessel extraction result from six candidates extracted from different threshold intervals.

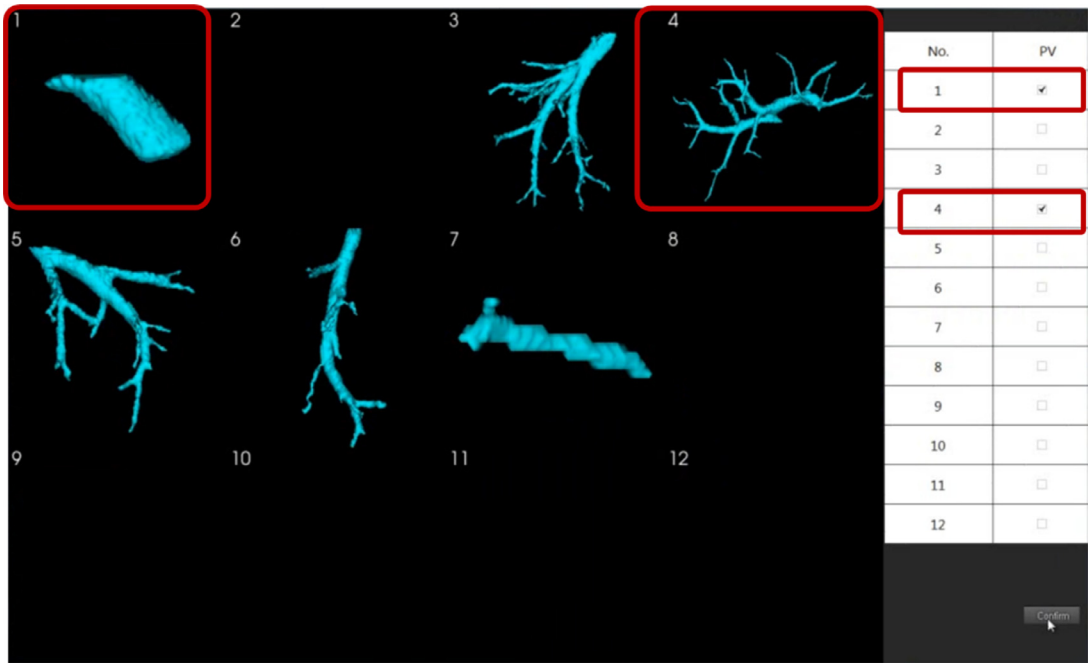

Fig. 8. An interface for the user to identify portal vein branches to separate portal vein and hepatic vein.

where $D(P_i)$ is distance between P_i and the picked point ($i = 1,\ldots,N$), $P_i \in \boldsymbol{V}$, is identified neighboring points of the picked point on the target PV branch $\boldsymbol{V}$. An interface (Fig. 9a) is provided for the user to sequentially pick up root points for the eight PV branches using the proposed local searching method. After all the root points are selected, the PV skeleton is automatically divided into eight branches by tracking each branch from its root point to the end of the branch and visualized with the rainbow color code (Fig. 9b). Lastly, in the liver segment classification stage, the liver is divided into eight segments by the NNA method. The NNA method [14,31] classifies a liver voxel into a segment if it has a shortest distance to the PV branches of that segment:

$$\mathrm{v} \in \mathrm{S}_i \text{ if } D_i(\mathrm{v}) = \min_{j=1,\ldots,8} \left\{ D_j(\mathrm{v}) \right\} \tag{2}$$

where $\mathbf{v}$ is a liver voxel, S_i represents a liver segment ($i = 1,\ldots,8$), and $D_j(\mathbf{v})$ is the Euclidean distance between the liver voxel $\mathbf{v}$ and a PV branch V_j ($j = 1,\ldots,8$). Fig. 9c illustrates classified liver segments by the NNA method.

3. Surgical planning method evaluation

3.1. Methods

3.1.1. Onsite evaluation of liver segmentation

The accuracy of liver segmentation was evaluated using five accuracy measures (volumetric overlap error: VOE, %; relative volume difference: RVD, %; average symmetric surface distance: ASD, mm; root mean square symmetric surface distance: RMSD, mm;

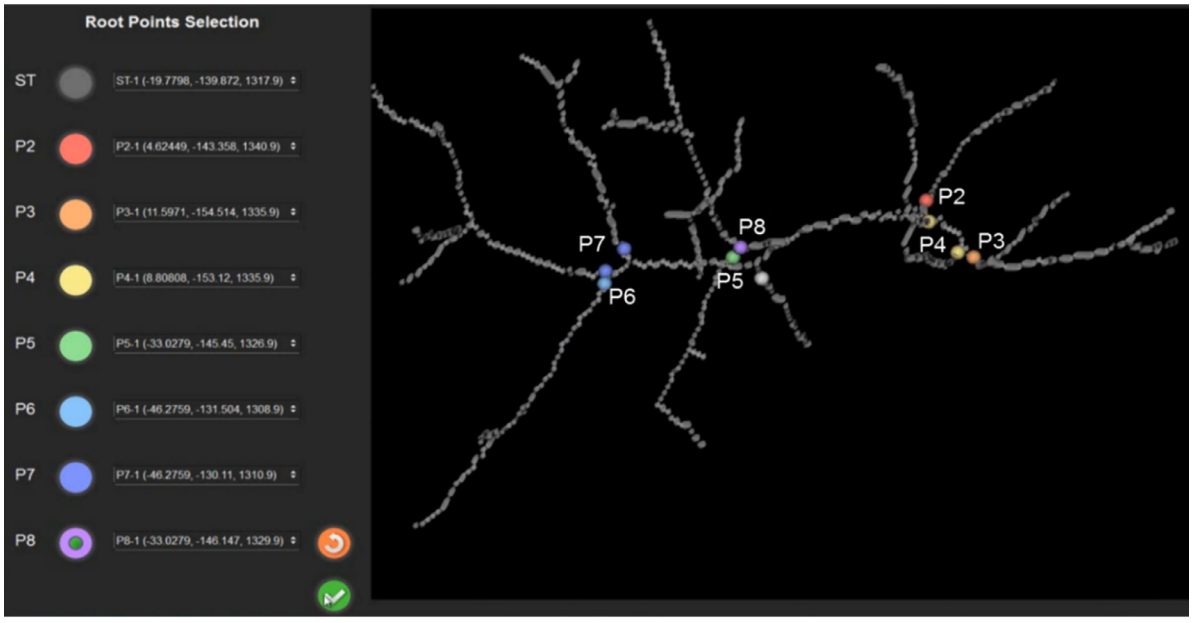

(a) Graphic user interface for root point selection

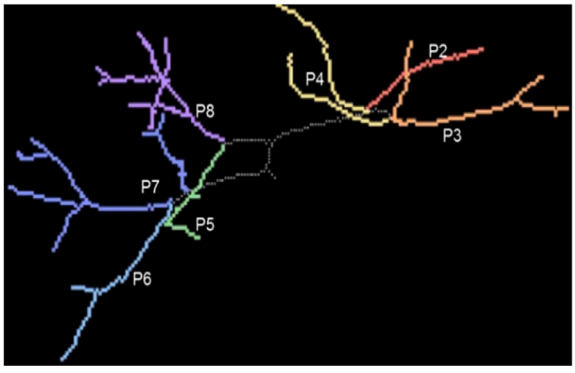

(b) Identified portal vein branches

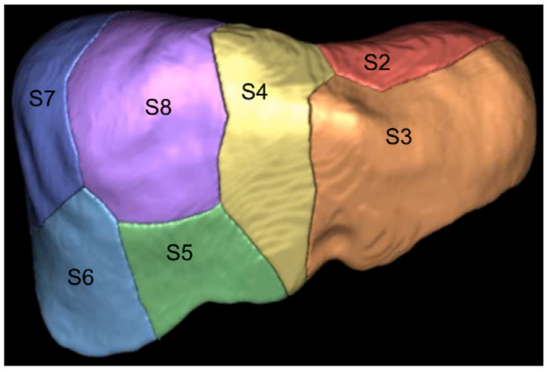

(c) Classification of liver segments

Fig. 9. Classification process of liver segments implemented in the present study.

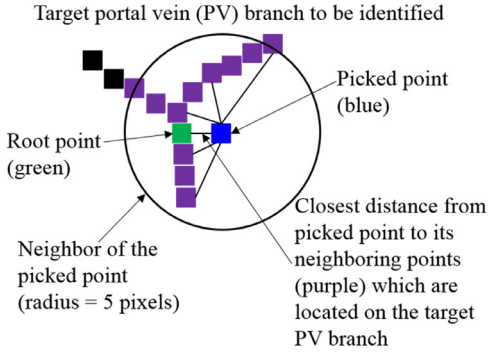

Fig. 10. A local searching method proposed in the present study for selection of a root point for portal vein branch identification.

maximum symmetric surface distance: MSD, mm) using a public liver database consisting of 20 training CT datasets and 10 test CT datasets (having tumors with different sizes in most cases, a slice thickness from 0.5 to 3.0 mm, and different contrast levels) provided by the SLIVER07 website. VOE is defined as the number of voxels outside the intersection of the extracted liver and the corresponding reference divided by the number of voxels in the union of the extracted liver and the reference [40,41]. RVD is defined as the difference between the extracted liver volume and the reference liver volume divided by the reference liver volume. ASD is defined as the average of minimal distances between the border of the extracted liver and the reference. RMSD is defined as the square root of the average squared distances between the border of the extracted liver and the reference. Lastly, MSD is defined as the maximum of all border voxel distances. A scoring system that combines the five metrics VOE, RVD, ASD, RMSD, and MSD into a single overall score [42] was provided by the SLIVER07 onsite evaluation website. The time of liver segmentation (s/CT dataset) was recorded to evaluate the efficiency of the liver segmentation method in this study on a computer with a CPU of 3.2 GHz.

3.1.2. Expert evaluation of vessel segmentation

The accuracy of vessel segmentation was evaluated in terms of false positive error, false negative error, and connections between PV and HV by an expert radiologist with the 10 public CT datasets provided by the SLIVER07 website. The radiologist was asked to visually detect false positive error, false negative error, and connections between PV and HV in the segmented vessel branches

Table 1
Onsite evaluation of liver segmentation from the SLIVER07 website.

Test case	VOE [%]	Score	RVD [%]	Score	ASD [mm]	Score	RMSD [mm]	Score	MSD [mm]	Score	Total Score
1	5.37	79.0	0.42	97.8	0.80	79.9	1.56	78.4	19.03	75.0	82.0
2	4.93	80.7	2.37	87.4	0.75	81.2	1.82	74.7	21.05	72.3	79.3
3	4.06	84.1	0.3	98.4	0.78	80.5	1.42	80.3	20.77	72.7	83.2
4	4.25	83.4	0.42	97.8	0.60	85.1	1.19	83.5	12.45	83.6	86.7
5	5.33	79.2	−0.05	99.7	0.95	76.2	1.91	73.5	25.18	66.9	79.1
6	4.74	81.5	−1.48	92.1	0.72	82.1	1.42	80.3	12.00	84.2	84.0
7	4.40	82.8	0.02	99.9	0.63	84.2	1.18	83.6	16.00	78.9	85.9
8	5.04	80.3	1.25	93.4	0.75	81.2	1.47	79.6	15.50	79.6	82.8
9	4.85	81.1	−0.41	97.8	0.57	85.7	0.91	87.3	17.49	77.0	85.8
10	4.64	81.9	−1.25	93.4	0.60	84.9	1.16	83.9	9.27	87.8	86.4
Average	4.76	81.4	0.16	95.8	0.72	82.1	1.40	80.5	16.87	77.8	83.5
S.D.	0.41	1.61	1.06	3.83	0.11	2.79	0.29	4.05	4.59	6.02	2.64

VOE: volumetric overlap error; RVD: relative volume difference; ASD: average symmetric surface distance; RMSD: root mean square symmetric surface distance; MSD: maximum symmetric surface distance; S.D.: standard deviation.

through an overlaid view of CT images with the segmented vessel branches. The time of vessel segmentation (min/CT dataset) was recorded to evaluate efficiency of the vessel segmentation method in this study.

3.1.3. Clinical evaluation of classification of liver segments

The accuracy of classification of liver segments was evaluated by liver graft volumetry accuracy and visual comparison of the classified segment boundaries with the intraoperative surgical cutting boundaries in LDLT. The liver graft volumetry accuracy was assessed in terms of absolute error (AE) defined as the absolute difference between the preoperatively estimated graft volume and intraoperatively calculated graft volume. Intraoperative graft volume was calculated as intraoperatively measured graft weight divided by liver density of 1.04 g/ml for the Korean population reported by Yu et al. [43]. Graft weight was intraoperatively measured after a liver graft was flushed by a surgeon at the back table with histidine–tryptophan–ketoglutarate solution (Custodiol; Köhler Chemie, Alsbach–Hähnlein, Germany) and trimmed. Pre-operative abdominal CT datasets and intra-operatively measured graft weights of 43 right-lobe donors (female = 11, male = 32; age = 27.2 ± 9.7 years) with normal livers from two medical centers were used for liver segment classification accuracy evaluation of the proposed method. The time of liver segment classification (min/CT dataset) was recorded to evaluate time efficiency of the liver segment classification method in this study.

3.2. Results

3.2.1. Onsite evaluation of liver segmentation

The average (± S.D.) values of VOE, RVD, ASD, RMSD, and MSD were 4.8% (± 0.4%), 0.2% (± 1.1%), 0.7 (± 0.1) mm, 1.4 (± 0.3) mm, and 16. 9 (± 4.6) mm as shown in Table 1. The average (± S.D.) value of overall score was 83.5 (± 2.6), ranked as the best automatic liver segmentation method. The average (± S.D.) liver extraction time of the proposed liver segmentation method was 55 (± 21) s/CT dataset. Fig. 11 shows liver segmentation results for relatively easy, average, and difficult cases.

3.2.2. Expert evaluation of vessel segmentation

No false positive errors were found in all the 10 CT datasets by the radiologist. False negative errors were found at distal branches due to small diameter and low contrast (Fig. 12). No connections between PV and HV were found in the 10 CT datasets (Fig. 13). The average (± S.D.) vessel extraction time of the proposed segmentation method was 2.0 (± 0.4) min/CT dataset.

3.2.3. Clinical evaluation of classification of liver segments

The proposed method showed high accuracy in liver graft volumetry (AE = 45.2 ± 20.9 ml; %AE = 6.8% ± 3.2%; percentage of %AE > 10% = 16.3%; percentage of %AE > 20% = none). The classified segment boundaries agreed with the intraoperative surgical cutting boundaries observed in a clinical environment (Fig. 14). The average (± S.D.) interaction time in classification of liver segments of the proposed method was 62 (± 9) s/CT dataset. The average (± S.D.) total time in classification of liver segments of the proposed method was 4.0 (± 0.7) min/CT dataset.

4. Discussion

4.1. Liver segmentation

The automatic liver segmentation method in this study overcomes the limitation of our previous hybrid semi-automatic method by adding a new feature of automatic identification of seed points. The previous hybrid semi-automatic method requires a user interaction period of about 30 s for selection of 40 seed points from 4 to 5 CT slices [12]. The automatic liver segmentation method in this study does not require any user interaction in the entire liver segmentation procedure by applying histogram analysis of intensity values and geometric analysis of the liver for automatic identification of seed points from 5 to 6 CT slices. Liver segmentation time is reduced by 22 s/CT dataset on average by the method in this study (average liver segmentation time = 55 s/CT dataset), compared to the hybrid semi-automatic method (average liver segmentation time = 77 s/CT dataset). The reduction of liver segmentation time would be beneficial for practical clinical applications such as a CT-guided hepatic ablation procedure which requires a fast liver segmentation for planning of ablation needle trajectory [9]. Liver segmentation accuracy is improved by 0.9% for volumetric overlap ratio in this study by adding a morphological closing procedure to include large vessel branches surrounded by liver tissue into segmentation results when compared to the hybrid semi-automatic method.

The proposed automatic liver segmentation method is accurate (average volumetric overlap radio = 95.2%) and efficient (average liver segmentation time = 55 s/CT dataset) to extract the liver from CT images. The comparison of our method with state-of-the-art methods using the 10 test CT datasets from the SLIVER07 website in terms of method type (e.g., interactive, semi- automatic, or automatic), total score, processing time, VOE, RVD, ASD, RMSD, and MSD was shown in Table 2. The proposed method showed better accuracy and time efficiency in liver segmentation than most of state-of-the-art methods. Beichel et al. [45]'s method is interactive which requires intensive manual editing (interaction time = 16 min/CT dataset) for the extracted liver. Six semi-

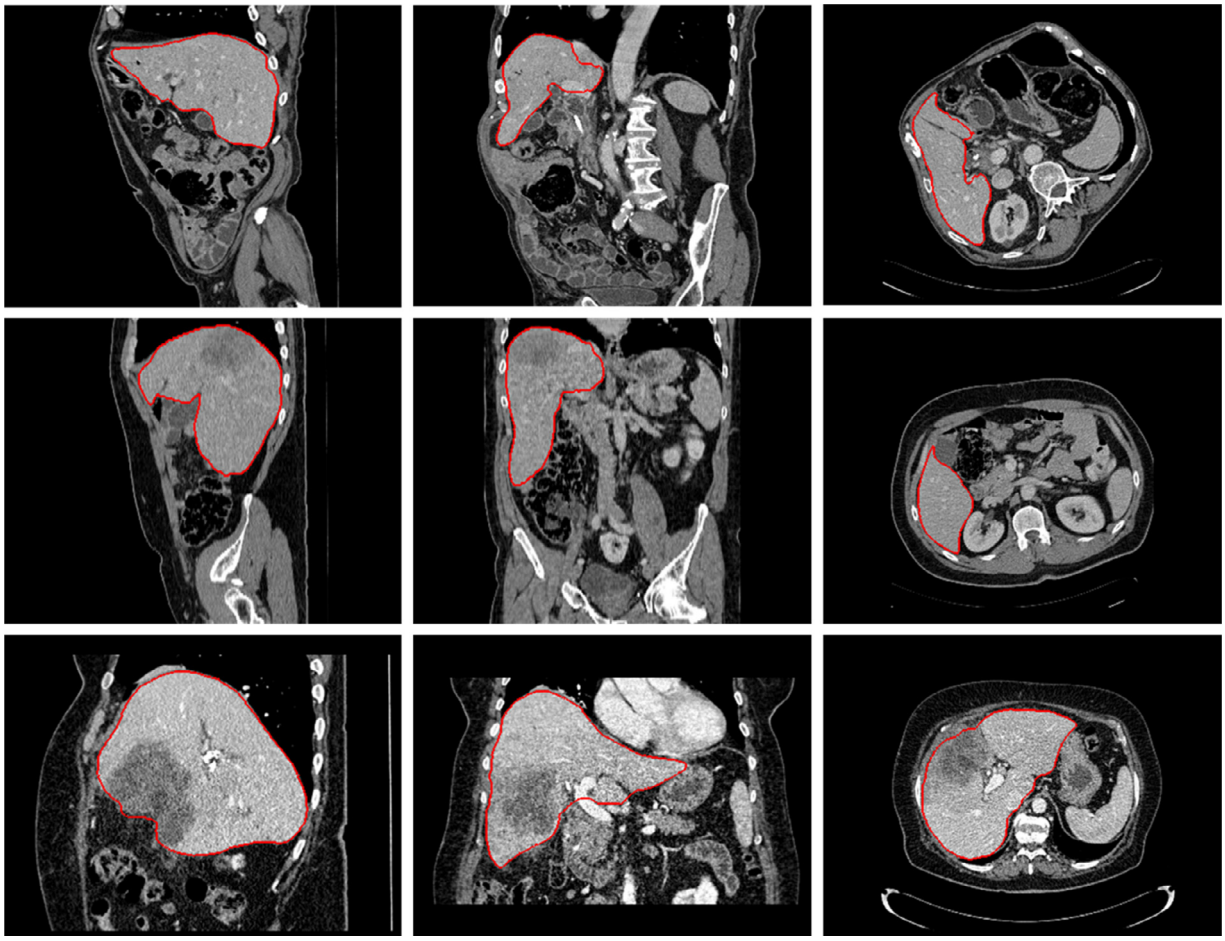

Fig. 11. Segmentation results by applying the automatic segmentation method proposed in this study (red) for three CT datasets (top to bottom: easy, average, and difficult cases; left to right: sagittal, coronal, and transversal slices) provided by the SLIVER07 website. (For interpretation of the references to color in this figure legend, the reader is referred to the web version of this article.)

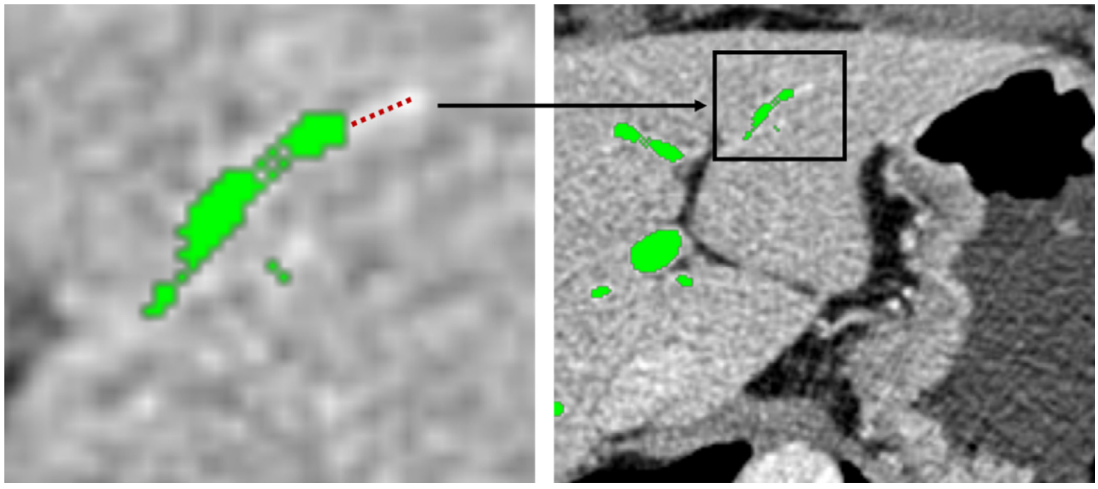

Fig. 12. A small missing branch (red dotted) at the distal part of a vessel tree (green) extracted by the vessel extraction method in this study. (For interpretation of the references to color in this figure legend, the reader is referred to the web version of this article.)

automatic methods including Maklad et al. [44]'s, Peng et al. [13]'s, Afifi & Nakaguchi [46]'s, Peng et al. [47]'s, Peng et al. [48]'s, and Wimmer et al. [50]'s require user's interaction for preparing seed points or regions, resulting in a longer liver segmentation time (2–9.7 min). Though Maklad et al.'s method achieved a better score than our method, it requires user interactions for the extraction of kidneys and vessels and separation of hepatic-and nonhepatic-vessels. Peng et al. [13]'s method showed a similar score to our method but a 3 times longer segmentation time than our method. Peng et al. [13] applied a multiregion-appearance based approach with graph cuts to extract the liver from a manual initialization of cylinders at different CT slices. The longer liver segmentation time in their method was caused by (1) computation cost of graph cuts method and (2) manual initialization of cylinders. Our method

Table 2
Comparison of the proposed liver segmentation method with state-of-the-art methods.

Method	Type	Score	Time [s]	VOE [%]	RVD [%]	ASD [mm]	RMSD [mm]	MSD [mm]
Maklad et al. [44]	Semi-automatic	85.7 ± 2.5	582	4.33 ± 0.69	0.28 ± 0.82	0.63 ± 0.15	1.19 ± 0.26	14.01 ± 2.73
Present study	Automatic	83.5 ± 2.6	55	4.76 ± 0.41	0.16 ± 1.06	0.72 ± 0.11	1.40 ± 0.29	16.87 ± 4.59
Peng et al. [13]	Semi-automatic	83.4 ± 3.1	120–180	4.58 ± 0.51	1.08 ± 0.80	0.68 ± 0.14	1.45 ± 0.36	16.88 ± 3.68
Beichel et al. [45]	Interactive	82.1 ± 2.8	2292	5.18 ± 0.89	0.96 ± 1.62	0.79 ± 0.18	1.43 ± 0.36	15.69 ± 3.30
Afifi & Nakaguchi [46]	Semi-automatic	81.7 ± 3.8	180	5.03 ± 0.87	1.83 ± 1.24	0.74 ± 0.16	1.52 ± 0.38	16.59 ± 3.89
Peng et al. [47]	Semi-automatic	80.6 ± 3.5	–	5.45 ± 0.82	1.03 ± 1.61	0.82 ± 0.14	1.68 ± 0.40	18.59 ± 4.31
Peng et al. [48]	Semi-automatic	80.0 ± 4.0	180	6.07 ± 1.13	− 0.04 ± 2.15	0.92 ± 0.23	1.61 ± 0.44	16.82 ± 2.32
Kainmuller et al. [49]	Automatic	77.3 ± 8.9	900	6.09 ± 2.02	− 2.86 ± 2.76	0.95 ± 0.33	1.87 ± 0.76	18.69 ± 8.02
Wimmer et al. [50]	Semi-automatic	76.8 ± 3.8	240–420	6.47 ± 0.92	1.04 ± 2.67	1.02 ± 0.16	2.0 ± 0.35	18.32 ± 4.66
Wu et al. [9]	Automatic	71.4 ± 5.9	27	7.87 ± 1.22	1.31 ± 2.96	1.29 ± 0.22	2.50 ± 0.68	23.56 ± 7.64

VOE: volumetric overlap error; RVD: relative volume difference; ASD: average symmetric surface distance; RMSD: root mean square symmetric surface distance; MSD: maximum symmetric surface distance.

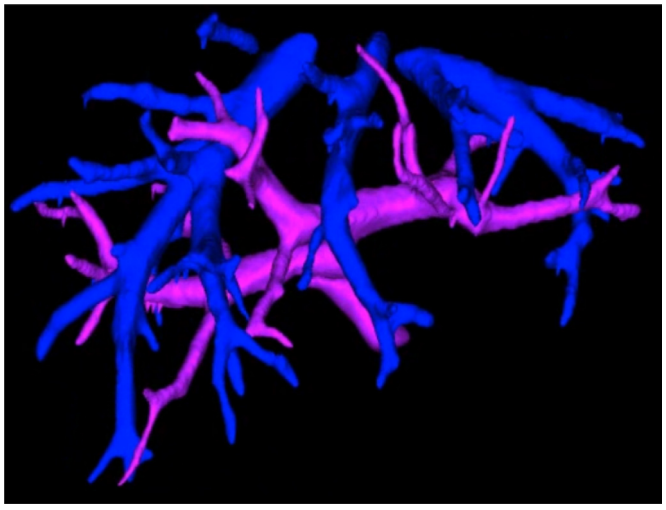

Fig. 13. Extracted portal vein (purple) and hepatic vein (blue) by applying the vessel extraction method proposed in this study. (For interpretation of the references to color in this figure legend, the reader is referred to the web version of this article.)

significantly increased liver segmentation efficiency through automatic identification of seed points while retaining sufficient accuracy. Two automatic methods including Kainmuller et al. [49]'s and Wu et al. [9]'s do not require any user interaction but sacrifice accuracy in liver segmentation. Kainmuller et al.'s method consists of a constrained free-form deformation method and a statistical shape model method based on a training set of 102 liver shapes. Wu et al. [9] applied supervoxel-based graph cuts to reduce computation expense in liver segmentation. Their method showed an inadequate segmentation at long and thin boundaries of the liver due to shrinking bias of graph cuts minimization. Furthermore, they generated seed points from only one CT slice (the largest liver slice), which is not enough for an accurate liver segmentation. Our method overcame the limitations of their method by (1) selecting 5 to 6 CT slices with an interval of 40 slices from whole CT volume and (2) sampling seed points in a 16×16 grid in each slice to avoid any inadequate segmentation. Furthermore, the proposed method sequentially incorporated a customized fast-marching level set method and a threshold-based level set method for providing accurate liver segmentation. The customized fast-marching level set method is able to generate an optimal initial liver region close to the true liver boundary in less than 10 s. The threshold-based level set method propagated the initial liver region to reach the true liver boundary for better accuracy in less than 40 s.

4.2. Vessel segmentation

The vessel segmentation method in this study showed no false positive errors or misconnections between PV and HV in the extracted vessel trees. The application of masking CT images with the extracted liver region excluded surroundings of the liver and therefore prevented false positive extraction of other vessels outside the liver. Furthermore, multiple extraction candidates of PV and HV from the six identified threshold intervals in this study

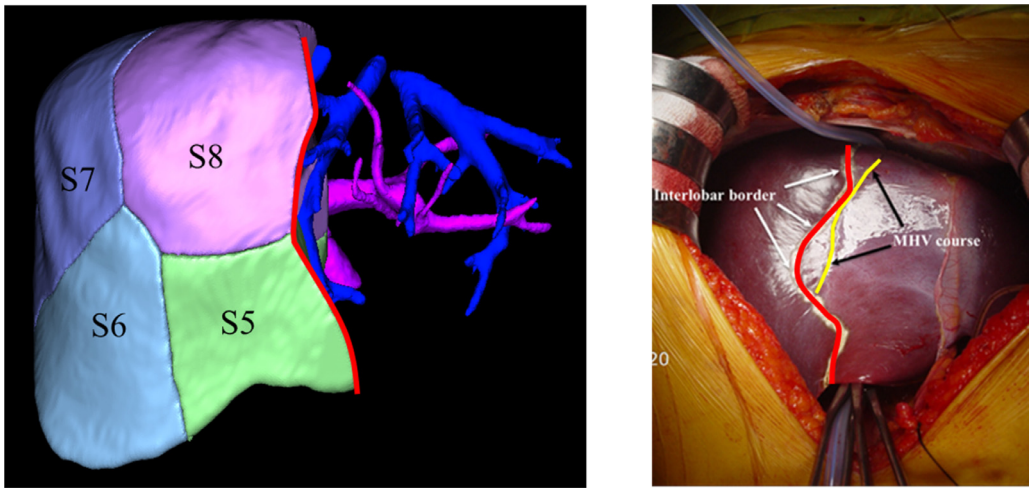

Fig. 14. Comparison of a classified boundary (red) by the method in this study to an intraoperative surgical cutting boundary (red) of left and right lobes for living donor liver transplantation. (For interpretation of the references to color in this figure legend, the reader is referred to the web version of this article.)

were provided for the user to select an appropriate extraction result and therefore prevented false positive extraction of liver tissues. A semi-automatic method based on connected component analysis was applied to separate PV and HV to prevent misconnections between PV and HV.

In PV and HV extraction stage, the method in this study required 10 to 30 s less user interaction time than semi-automatic methods [16,17] by automatic identification of seed points through histogram analysis of intensity values. However, in PV and HV separation stage, for a worst case where PV and HV branches are heavily connected with each other, our semi-automatic separation method may require an intensive user interaction to separate PV and HV. As a future work, a more advanced method based on histogram analysis, geometrical analysis, and graph cuts [15,20] needs to be developed or implemented for automatic separation of PV and HV.

4.3. Liver segment classification

In this study, we developed a local searching method for selection of a root point on a target PV branch to assign the branch to its corresponding liver segment. Even though a false point is picked due to a lack of depth perception, the local searching method can correctly detect the root point through searching neighboring points around the picked point. User interaction time in identification of eight PV branches is significantly reduced by selecting root points with the local searching method (user interaction time = 1 min), compared to selecting root points without using the local searching method (user interaction time = 20 min). Beichel et al. [31] applied augmented reality (AR) techniques to selection of points in an AR environment for identification of PV branches using tracked input devices and see-through head mounted displays. In the AR environment, depth information can be perceived so that a point can be selected like in a real 3D world. However, the performance of the AR technique was not evaluated and discussed in Beichel et al. [31]'s study. Compared to their method, our method can help correct and efficient selection of a point even under a lack of depth perception condition. Furthermore, our method is more accessible than Beichel et al. [31]'s method since we do not require any extra equipment.

The present study verified the accuracy of classification of liver segments in terms of liver graft volumetry accuracy and visual comparison of the classified boundaries to the surgical cutting boundaries in a clinical environment. The proposed method showed high accuracy in liver graft volumetry ($AE = 45.2 \pm 20.9$ ml; $\%AE = 6.8\% \pm 3.2\%$; percentage of $\%AE > 10\% = 16.3\%$; percentage of $\%AE > 20\%$ = none) and the classified boundaries were found agreeing with the intraoperative surgical cutting boundaries.

The present study tested the proposed segmentation methods for liver and its vessels using the 10 test CT datasets from the SLIVER07 website. Though the 10 CT datasets are different from each other (e.g., having tumors with different sizes in most cases, a slice thickness from 0.5 to 3.0 mm, and different contrast levels), testing our methods with more CT datasets from multiple medical centers needs to be conducted as a future work.

The applicability of the proposed surgical planning method to abdominal images of magnetic resonance imaging (MRI) needs to be examined as a future work. Though CT images are still mainly used as a routine clinical examination, MRI images are becoming a preferred procedure due to having advantages (e.g., no radiation and available for bile duct analysis). We have tried to apply our proposed method to segmentation of liver, vessels, and bile duct from MRI images as a pilot experiment and obtained promising results after adjusting parameter values.

Conflict of interest

No conflict of interest.

Acknowledgments

This study was jointly supported by Fund of Biomedical Research Institute, Chonbuk National University Hospital, Korea and Basic Science Research Program through the National Research Foundation of Korea (NRF) funded by the Ministry of Education (NRF-2017R1D1A1B03036081). Drs. Heecheon You and Hee Chul Yu contributed equally to this work.

References

[1] O.A. Catalano, A.H. Singh, R.N. Uppot, P.F. Hahn, C.R. Ferrone, D.V. Sahani, Vascular and biliary variants in the liver: implications for liver surgery, Radiographics 28 (2008) 359–378.
[2] H.P. Meinzer, M. Thorn, E. Carlos, Computerized planning of liver surgery – an overview, Comput. Graphics 26 (2002) 569–576.
[3] A. Radtke, S. Nadalin, G.C. Sotiropoulos, E.P. Molmenti, T. Schroeder, C. Valentin-Gamazo, H. Lang, M. Bockhorn, H.O. Peitgen, C.E. Broelsch, M. Malagó, Computer-assisted operative planning in adult living donor liver transplantation: a new way to resolve the dilemma of the middle hepatic vein, World J. Surg. 31 (2007) 175–185.
[4] S. Satou, Y. Sugawara, S. Tamura, Y. Kishi, J. Kaneko, Y. Matsui, N. Kokudo, M. Makuuchi, Three dimensional computed tomography for planning donor hepatectomy, Transpl. Proc. 39 (2007) 145–149.
[5] P. Limanond, S.S. Raman, R.M. Ghobrial, R.W. Busuttil, D.S. Lu, Preoperative imaging in adult-to-adult living related liver transplant donors: what surgeons want to know, J. Comput. Assist. Tomogr. 28 (2004) 149–157.
[6] N. Mugunthan, D. Jansirani, C. Felicia, J. Anbalagan, Anatomical variations in the arterial supply of liver, Int. J. Anat. Var. 5 (2012) 107–109.
[7] L. Ruskó, G. Bekes, G. Németh, M. Fidrich, Fully automatic liver segmentation for contrast-enhanced CT images, in: Proc. MICCAI Workshop 3-D Segmentat. Clinic: A Grand Challenge, 2007, pp. 143–150.
[8] M. Ciecholewski, Automatic liver segmentation from 2D CT images using an approximate contour model, J. Sign. Process. Syst. 74 (2014) 151–174.
[9] W. Wu, Z. Zhou, S. Wu, Y. Zhang, Automatic liver segmentation on volumetric CT images using supervoxel-based graph cuts, Comput. Math. Methods Med. (2016) 14 pages. http://dx.doi.org/10.1155/2016/9093721.
[10] O. Zayane, B. Jouini, M.A. Mahjoub, Automatic liver segmentation method in CT images, Can. J. Image Proc. Comput. Vis. 2 (2011) 92–95.
[11] N.H. Abdel-massieh, Fully automatic technique for liver segmentation from abdominal CT scan with knowledge-based constraints, in: L. Saba (Ed.), Computed Tomography - Clinical Applications, InTech, Rijeka, 2012, pp. 195–210.
[12] X. Yang, H.C. Yu, Y. Choi, W. Lee, B. Wang, J. Yang, H. Hwang, J.H. Kim, J. Song, B.H. Cho, H. You, A hybrid semi-automatic method for liver segmentation based on level-set methods using multiple seed points, Comput. Methods Programs Biomed. 113 (2014) 69–79.
[13] J. Peng, P. Hu, F. Lu, Z. Peng, D. Kong, H. Zhang, 3D liver segmentation using multiple region appearances and graph cuts, Med.Phys. 42 (2015) 6840–6852.
[14] D. Selle, B. Preim, A. Schenk, H.O. Peitgen, Analysis of vasculature for liver surgical planning, IEEE Trans. Med. Imag. 21 (2002) 1344–1357.
[15] S. Esneault, C. Lafon, J.-L. Dillenseger, Liver vessels segmentation using a hybrid geometrical moments/graph cuts method, IEEE Trans. Biomed. Eng. 57 (2010) 276–283.
[16] J. Yi, J.B. Ra, A locally adaptive region growing algorithm for vascular segmentation, Int. J. Imaging Syst. Technol. 13 (2003) 208–214.
[17] L.M. Lorigo, O.D. Faugeras, W.E.L. Grimson, R. Keriven, R. Kikinis, A. Nabavi, C.-F. Westin, CURVES: curve evolution for vessel segmentation, Med. Image Anal. 5 (2001) 195–206.
[18] L. Soler, H. Delingette, G. Malandain, J. Montagnat, N. Ayache, C. Koehl, O. Dourthe, B. Malassagne, M. Smith, D. Mutter, J. Marescaux, Fully automatic anatomical, pathological, and functional segmentation from CT scans for hepatic surgery, Comput. Aid. Surg. 6 (2001) 131–142.
[19] O.C. Eidheim, L. Aurdal, T. Omholt-Jensen, T. Mala, B. Edwin, Segmentation of liver vessels as seen in MR and CT images, Int. J. Comput. Assisted Radiol. Surg. 1268 (2004) 201–206.
[20] C. Bauer, T. Pock, E. Sorantin, H. Biscof, R. Beichel, Segmentation of interwoven 3D tubular tree structures utilizing shape priors and graph cuts, Med. Image Anal. 14 (2010) 172–184.
[21] E. Goceri, Automatic labeling of portal and hepatic veins from MR images prior to liver transplantation, Int. J. Comput. Assisted Radiol. Surg. 11 (2016) 2153–2161.
[22] E. Goceri, Z.K. Shah, M.N. Gurcan, Vessel segmentation from abdominal magnetic resonance images: adaptive and reconstructive approach, Int. J. Numer. Methods Biomed. Eng. 33 (2016) e2811.
[23] E. Gočeri, in: A comparative evaluation for liver segmentation from SPIR images and a novel level set method using signed pressure force function, İzmir Institute of Technology, 2013, pp. 1–161.

[24] J. Domingo, E. Dura, E. Gočeri, Iteratively learning a liver segmentation using probabilistic atlases: preliminary results, in: Proc. 15th IEEE International Conference on Machine Learning and Applications (ICMLA), 2016, pp. 593–598.
[25] E. Goceri, M.Z. Unlu, C. Guzelis, O. Dicle, An automatic level set based liver segmentation from MRI data sets, in: Proc. Image Processing Theory, 3rd International Conference on Tools and Applications (IPTA), 2013, pp. 192–197.
[26] E. Goçeri, M.N. Gürcan, O. Dicle, Fully automated liver segmentation from SPIR image series, Comput. Biol. Med. 53 (2014) 265–278.
[27] H.-P. Meinzer, M. Thorn, C. Cárdenas, Computerized planning of liver surgery - an overview, Comput. Graphics 26 (2002) 569–576.
[28] L. Soler, H. Delingette, G. Malandain, J. Montagnat, N. Ayache, C. Koehl, O. Dourthe, B. Malassagne, M. Smith, D. Mutter, J. Marescaux, Fully automatic anatomical, pathological, and functional segmentation from CT scans for hepatic surgery, Comput. Aid. Surg. 6 (2001) 131–142.
[29] D.A. Oliveira, R.Q. Feitosa, M.M. Correia, Segmentation of liver, its vessels and lesions from CT images for surgical planning, Biomed. Eng. Online 10 (2011) 23 pages. http://dx.doi.org/10.1186/1475-925X-10-30.
[30] C. Couinaud, Le foie: Etudes anatomiques Et Chirurgicales, Masson, Paris, 1957.
[31] R. Beichel, T. Pock, C. Janko, R.B. Zotter, B. Reitinger, A. Bornik, K. Palágyi, E. Sorantin, G. Werkgartner, H. Bischof, M. Sonka, Liver segment approximation in CT data for surgical resection planning, Proc. SPIE Conf. Med. Imag. 5370 (2004) 1435–1446.
[32] L. Ibáñez, W. Schroeder, L. Ng, J. Cates, The ITK Software Guide, 2nd, Kitware Inc., 2005.
[33] J.A. Sethian, A fast marching level set method for monotonically advancing fronts, in: Proc. Natl. Acad. Sci., 1996, pp. 1591–1595.
[34] C.-Y. Hsu, C.-H. Yang, H.C. Wang, Multi-threshold level set model for image segmentation, EURASIP J. Adv. Signal Process. (2010) 8 pages. http://dx.doi.org/10.1155/2010/950438.
[35] A. Lefohn, J. Cates, R. Whitaker, Interactive, GPU-based level sets for 3D segmentation, in: Proc. Medical Image Computing and Computer Assisted Intervention (MICCAI), 2878, Lecture Notes in Computer Science, 2003, pp. 564–572.
[36] L. Vincent, Morphological transformations of binary images with arbitrary structuring elements, Signal Process. 22 (1991) 3–23.
[37] N. Nikopoulos, I. Pitas, An efficient algorithm for 3D binary morphological transformations with 3D structuring elements of arbitrary size and shape, in: Proc. IEEE Workshop on Nonlinear Signal and Image Processing, 1997.
[38] G. Lehmann, Binary morphological closing and opening image filters, Insight J. (2005). http://hdl.handle.net/1926/141.
[39] H. Homann, Implementation of a 3D thinning algorithm, Insight J. (2007). http://hdl.handle.net/1926/1292.
[40] C. Muramatsu, T. Nakagawa, A. Sawada, Y. Hatanaka, T. Hara, T. Yamamoto, H. Fujita, Automated segmentation of optic disc region on retinal fundus photographs: aomparison of contour modeling and pixel classification methods, Comput. Methods Programs Biomed. 101 (2011) 23–32.
[41] S. Ghose, A. Oliver, R. Marti, X. Llado, J.C. Vilanova, J. Freixenet, J. Mitra, D. Sidibe, F. Meriaudeau, A survey of prostate segmentation methodologies in ultrasound, magnetic resonance and computed tomography images, Comput. Methods Programs Biomed. 108 (2012) 262–287.
[42] T. Heimann, B. van Ginneken, M. Styner, Y. Arzhaeva, V. Aurich, C. Bauer, A. Beck, C. Becker, R. Beichel, G. Bekes, F. Bello, G. Binnig, H. Bischof, A. Bornik, P. Cashman, Y. Chi, A. Cordova, B. Dawant, M. Fidrich, J. Furst, D. Furukawa, L. Grenacher, J. Hornegger, D. Kainmuller, R. Kitney, H. Kobatake, H. Lamecker, T. Lange, J. Lee, B. Lennon, R. Li, S. Li, H-P. Meinzer, G. Nemeth, D. Raicu, A-M. Rau, E. van Rikxoort, M. Rousson, L. Rusko, K. Saddi, G. Schmidt, D. Seghers, A. Shimizu, P. Slagmolen, E. Sorantin, G. Soza, R. Susomboon, J. Waite, A. Wimmer, I. Wolf, Comparison and evaluation of methods for liver segmentation from CT datasets, IEEE Trans. Med. Imag. 28 (2009) 1251–1265.
[43] H.C. Yu, H. You, H. Lee, Z.W. Jin, J.I. Moon, B.H. Cho, Estimation of standard liver volume for liver transplantation in the Korean population, Liver Transpl. 10 (2004) 779–783.
[44] A.S. Maklad, M. Matsuhiro, H. Suzuki, Y. Kawata, N. Niki, M. Satake, N. Moriyama, T. Utsunomiya, M. Shimada, Blood vessel-based liver segmentation using the portal phase of an abdominal CT dataset, Med. Phys. 40 (2013) 113501 18pp.
[45] R. Beichel, C. Bauer, A. Bornik, E. Sorantin, H. Bischof, Liver segmentation in CT data: a segmentation refinement approach, in: Proc. 3D Segmentation in the Clinic: A Grand Challenge, 2007, pp. 235–245.
[46] A. Afifi, T. Nakaguchi, Liver segmentation approach using graph cuts and iteratively estimated shape and intensity constrains, Proc. Med. Image Comput. Comput. Assisted Intervention 2 (2012) 395–403.
[47] J. Peng, Y. Wang, D. Kong, Liver segmentation with constrained convex variational model, Pattern Recognit. Lett. 43 (2014) 81–88.
[48] J. Peng, F. Dong, Y. Chen, D. Kong, A region-appearance based adaptive variational model for 3D liver segmentation, Med. Phys. 41 (2014) 043502 11pp.
[49] D. Kainmuller, T. Lange, H. Lamecker, Shape constrained automatic segmentation of the liver based on a heuristic intensity model, in: Proc. MICCAI Workshop 3D Segmentat. Clinic: A Gand Challenge, 2007, pp. 109–116.
[50] A. Wimmer, G. Soza, J. Hornegger, A generic probabilistic active shape model for organ segmentation, Proc. Med. Image Comput. Comput. Assisted Intervention 1 (2009) 26–33.